

Finding dominant transition pathways via global optimization of action

Juyong Lee*

*Laboratory of Computational Biology,
National Heart, Lung, and Blood Institute (NHLBI),
National Institutes of Health (NIH), Bethesda, Maryland 20892, U.S.A.*

In-Ho Lee

Korea Research Institute of Standards and Science, Daejeon 34113, Republic of Korea

InSuk Joung and Jooyoung Lee

School of Computational Sciences, Korea Institute of Advanced Study, Seoul 02455, Korea

Bernard R. Brooks

*Laboratory of Computational Biology,
National Heart, Lung, and Blood Institute (NHLBI),
National Institutes of Health (NIH), Bethesda, Maryland 20892, USA*

(Dated: April 24, 2022)

Abstract

We present a new computational approach, Action-CSA, to sample multiple reaction pathways with fixed initial and final states through global optimization of the Onsager-Machlup action using the conformational space annealing method. This approach successfully samples not only the most dominant pathway but also many other possible paths without initial guesses on reaction pathways. Pathway space is efficiently sampled by crossover operations of a set of paths and preserving the diversity of sampled pathways. The sampling ability of the approach is assessed by finding pathways for the conformational changes of alanine dipeptide and hexane. The benchmarks demonstrate that the rank order and the transition time distribution of multiple pathways identified by the new approach are in good agreement with those of long molecular dynamics simulations. We also show that the lowest action folding pathway of the mini-protein FSD-1 identified by the new approach is consistent with previous molecular dynamics simulations and experiments.

PACS numbers: 87.15.ap,87.15.hm,87.15.hp,82.30.Qt,82.20.Wt

Finding multiple reaction pathways between two end states remains a challenging problem in computational biophysics [1]. For this purpose, performing a long-time molecular dynamics (MD) simulation is a commonly used approach. Despite recent progress in the methodologies of MD, this approach still suffers from a timescale problem. Many biological reactions such as protein folding and conformational transitions occur in the microsecond or millisecond ranges, which are costly with conventional computers. In addition, MD simulations starting from one end state are not guaranteed to reach the other end state of interest. Thus developing an efficient computational method to find multiple possible reaction pathways connecting two end states is necessary. There are currently no practical methods that can efficiently produce the multiple dominant pathways connecting two well-defined end point states in a complex system. The objective of this work is to present such a method. Other approaches using a conformational driving force do not sample alternatives. Methods that are robust, such as transition path sampling [2, 3], are very expensive to use for complex systems in the presence of multiple steps and barriers.

Various chain-of-state methods have been suggested based on the assumption that a dominant transition pathway between two states follows the minimum energy pathway [4–6]. The limitations of these methods are that they do not consider the dynamics of a system and find only the nearest local minimum solution from a given initial pathway [1]. Alternative methods based on the principle of least action have been suggested [7–13]. Passerone and Parrinello suggested the action-derived molecular dynamics (ADMD) method based on the combination of classical action and a penalty term that conserves the total energy of a system [11, 12]. To enhance the convergence of ADMD calculations, Lee et al. introduced a kinetic energy penalty term based on the equipartition theorem [13–16]. Although ADMD yields physically relevant pathways, it has two practical limitations [13, 17]: i) it strongly depends on the initial guess of a pathway; and ii) it cannot identify the most dominant pathway when there are multiple pathways because the classical least action principle is an extremum principle.

For diffusive processes, the second problem can be avoided by using the Onsager-Machlup (OM) action S_{OM} [8, 18–23]. Onsager and Machlup showed that the relative probability to observe a pathway with an OM action of S is proportional to $e^{-S/k_{\text{B}}T}$ where k_{B} is the Boltzmann constant and T is a temperature. Thus the most dominant pathway corresponds to the one that minimizes S_{OM} and the same result can be obtained by solving the Fokker-

Planck equation [24–26]. This property recasts the problem of finding dominant pathways into a global optimization problem. However, finding the global minimum of S_{OM} is a numerically challenging task because the minimization of S_{OM} requires the second derivatives of a potential function, which are computationally expensive, at best, and wholly unavailable for many quantum mechanical energy surfaces.

In this work, we propose an efficient computational method that finds not only the most dominant pathway but also multiple suboptimal pathways without second derivative calculations. For global optimization of S_{OM} , we used an efficient global optimization method called conformational space annealing (CSA) based on a combination of genetic algorithm, simulated annealing, and Monte Carlo minimization [27, 28]. The CSA method has been demonstrated to be extremely efficient in solving various global optimization problems including finding low energy conformations of Lennard-Jones clusters [29], protein structure prediction [28–35], and community detection in networks [36–38]. CSA is the most robust method available in CHARMM [39, 40] for generating low energy conformations of peptides. We extend the CSA approach to examining pathways, preserving all features that make it robust and efficient, by applying it to sets of entire pathways represented as a chain-of-states. From benchmark simulations using alanine dipeptide, we observed that our method finds multiple transition pathways, which are consistent with long-time Langevin dynamics (LD) simulations. In addition, the rank order statistics and transition time distributions of the multiple transition pathways are in good agreement with those of the LD results. We will call the method Action-CSA.

Here, we briefly review the theoretical background behind Action-CSA. If a system with N atoms with a potential energy V follows the overdamped Langevin dynamics,

$$\gamma \mathbf{m} \dot{\mathbf{x}} = -\frac{\partial V}{\partial \mathbf{x}} + \mathbf{R}, \quad (1)$$

where \mathbf{m} is a diagonal mass matrix, \mathbf{x} is a $3N$ dimensional coordinate vector, γ is collision frequency, and \mathbf{R} is a Gaussian random force, the relative probability of finding a final state \mathbf{x}_f at a time t from an initial state \mathbf{x}_i via diffusive trajectories $\mathbf{x}(t)$ is determined by using the path integral approach and OM action $S_{\text{OM}}[\mathbf{x}(t)]$ [18, 19]:

$$P(\mathbf{x}_f|\mathbf{x}_i; t) = \int_0^t \mathcal{D}\mathbf{x}(t) \exp\left(-\frac{S_{\text{OM}}[\mathbf{x}(t)]}{k_{\text{B}}T}\right), \quad (2)$$

where $\mathcal{D}\mathbf{x}(t)$ indicates that the integration runs over all possible pathways $\mathbf{x}(t)$. This relationship suggests that if the S_{OM} values of all physically accessible pathways are obtained,

one can determine the relative populations of multiple pathways. Thus, S_{OM} is a proper target objective function of global optimization. The generalized OM action of a pathway $\mathbf{x}(t)$ is defined [18, 19, 41, 42]:

$$S_{\text{OM}}[\mathbf{x}(t)] = \frac{\Delta V}{2} + \frac{1}{4\gamma} \int_0^t d\tau \{[\gamma \mathbf{m}\dot{\mathbf{x}}(\tau)]^2 + \|\nabla V[\mathbf{x}(\tau)]\|^2 - 2k_{\text{B}}T\nabla^2 V[\mathbf{x}(\tau)]\}, \quad (3)$$

where $\Delta V = V(\mathbf{x}_{\text{f}}) - V(\mathbf{x}_{\text{i}})$. The last term is related to trajectory entropy connected with fluctuations [42–44] and was not presented in the original work by Onsager and Machlup because the harmonic potential was considered [18, 19]. Note that the minimization of S_{OM} using analytic local minimization algorithms requires third derivatives. This makes the direct global optimization of S_{OM} hard to be applied to detect transition pathways of biomolecules with all-atom force fields due to the complexity of implementation and high computational cost. For numerical calculations based on a chain-of-state representation, the OM action should be discretized. The method uses the second-order discretization of the symmetric OM formula, which uses only gradients for S_{OM} calculations [45]:

$$S_{\text{OM}}[\mathbf{x}(t)] = \frac{\Delta V}{2} + \sum_{i=0}^{P-1} \frac{\Delta t}{4\gamma} \left\{ \left[\frac{\gamma \mathbf{m}(\mathbf{x}_{i+1} - \mathbf{x}_i)}{\Delta t} \right]^2 + \frac{\|\nabla V(\mathbf{x}_i)\|^2 + \|\nabla V(\mathbf{x}_{i+1})\|^2}{2} - \frac{\gamma \mathbf{m}(\mathbf{x}_{i+1} - \mathbf{x}_i)}{\Delta t} [\nabla V(\mathbf{x}_{i+1}) - \nabla V(\mathbf{x}_i)] \right\}, \quad (4)$$

where $P + 1$ is the number of replicas, Δt is a time step between successive replicas, and $t = P\Delta t$ is the total transition time. This formula is more efficient than the direct implementation of Eq. (3) since it requires only the first derivatives of V to evaluate S_{OM} .

Here, we describe the application of CSA to optimize S_{OM} . In general, a pathway is represented as a chain of $P - 1$ replicas with N atoms for each replica leading to $3N(P - 1)$ total degrees of freedom. Each replica is represented by a sequence of $3N - 6$ internal dihedral angles and 6 net translational/rotational degrees of freedom. An Action-CSA calculation starts with a set of random pathways on a pathway space. Subsequently, the actions of the random pathways should be locally optimized. We call this set of pathways a bank, and update conformations in the bank during the Action-CSA calculation. As stated previously, direct minimization of S_{OM} using analytic gradients is computationally challenging.

For a computationally feasible local action optimization, we optimized a pathway using

a modified action from ADMD instead of using S_{OM} . The discretized classical action is defined:

$$S_{\text{classical}}[\mathbf{x}(t)] = \sum_{i=0}^{P-1} L_i(\mathbf{x}_i) \Delta t = \sum_{i=0}^{P-1} \left[\frac{\mathbf{m}(\mathbf{x}_i - \mathbf{x}_{i+1})^2}{2\Delta t^2} - V(\mathbf{x}_i) \right] \Delta t. \quad (5)$$

Physically accessible pathways correspond to the stationary points of $S_{\text{classical}}$. Finding such pathways is a computationally difficult task because $S_{\text{classical}}$ is not bounded; $S_{\text{classical}}$ can be minimized or maximized, and the stationary points of $S_{\text{classical}}$ can be minima, maxima or saddle points. Another practical problem is that the total energies of pathways satisfying the stationary condition $\delta S_{\text{classical}} = 0$ may not be conserved [11]. To find pathways that satisfy the principle of least action and conserve total energies, a modified action with a penalty term restraining total energy was suggested [11]:

$$\begin{aligned} \Theta(\mathbf{x}_i; E) &= \mu_A S_{\text{classical}} + \mu_E \sum_{i=0}^{P-1} (E_i - E)^2 \\ &= \mu_A \sum_{i=0}^{P-1} \left[\frac{\mathbf{m}(\mathbf{x}_i - \mathbf{x}_{i+1})^2}{2\Delta t^2} - V(\mathbf{x}_i) \right] \Delta t + \mu_E \sum_{i=0}^{P-1} \left\{ \left[\frac{\mathbf{m}(\mathbf{x}_i - \mathbf{x}_{i+1})^2}{2\Delta t^2} + V(\mathbf{x}_i) \right] - E \right\}^2, \end{aligned} \quad (6)$$

where E is a targeted total energy of a system, μ_A and μ_E are the weighting parameters of the classical action, and the restraint term for energy conservation. The minimization of $\Theta[\mathbf{x}(t); E]$ requires only the first derivatives of V .

We call the set of locally optimized initial random pathways using $\Theta[\mathbf{x}(t); E]$ the *first bank*. The first bank remains the same throughout the optimization and is used as the reservoir of partially optimized pathways to enhance the diversity of pathway search. A copy of the first bank is generated and called a *bank*. The conformations in the bank are updated during a calculation while the size of the bank is kept constant. By using the pathways included in the first bank and the bank, new trial pathways are generated by performing crossover and random perturbation operations. For a crossover operation, two pathways, a seed pathway from the bank and a random pathway either from the bank or the first bank, are selected and random parts of two selected configurations are swapped. For a random perturbation, a certain number of degrees of freedom of a seed pathway, up to 5% of total degrees of freedom, were randomly changed. The generated trial pathways are

locally optimized using $\Theta[\mathbf{x}(t); E]$ to remove any possible artifacts generated by the crossover and the random perturbation operations. However, after local minimizations, the bank was updated by comparing the S_{OM} values of the existing pathways and the new ones instead of $\Theta[\mathbf{x}(t); E]$.

A key feature of CSA is a sophisticated bank-update procedure that prevents a search being trapped in local minima during the optimization and keeps the diversity of the bank. For a newly obtained configuration α , the distances between α and the existing ones in the bank are calculated. If the distance D between α and its closest neighbor is less than a cutoff distance D_{cut} , only the better configuration in terms of the objective function is selected. If $D > D_{\text{cut}}$, α is considered a new configuration and it replaces the worst configuration in the bank. At initial stages of a calculation, D_{cut} is kept large for wider sampling. As the calculation proceeds, it gradually decreases for a refined search near the global minimum. The bank keeps updating until no pathway with a lower S_{OM} is found. In this work, a distance between two pathways was measured by the Fréchet distance [46]. More details on a general CSA procedure are described elsewhere [27–29, 32, 34, 35].

To verify that Action-CSA successfully finds multiple transition pathways and allows one to determine the rank order of the pathways based on their optimized S_{OM} values, we applied our method to investigate the conformational transition of alanine dipeptide from $C7_{\text{eq}}$ to $C7_{\text{ax}}$ in the vacuum. Here, we used the polar hydrogen representation in the PARAM19 force field [47] and dielectric constant was set to 1.0 [48]. We performed Action-CSA simulations with different transition times, t in Eqs. (4) and (6), ranging from 0.2 ps to 2.0 ps with an interval of 0.1 ps. The numbers of replicas were adjusted with t to keep the time step between replicas $\Delta t = 5$ fs. All simulations were performed at temperature $T = 350$ K with a collision frequency $\gamma = 1.0$ ps⁻¹. The reference total energy E in Eq. (5) was obtained by adding the initial potential energy $V(\mathbf{x}_i) = -43.3$ kcal/mol and a kinetic energy of 12.5 kcal/mol estimated by $3Nk_{\text{B}}T/2$ with the number of atoms $N = 12$. The weighting parameters μ_A and μ_E in Eq. (5) were set to -1.0 and 1.0 , respectively. For comparison purposes, we performed 500 μs LD simulations of alanine dipeptide under the same condition and counted the number of the $C7_{\text{eq}} \rightarrow C7_{\text{ax}}$ transitions.

Now we will show that the Action-CSA identifies not only the most dominant pathway but also multiple possible pathways. We identified 8 different pathways for the $C7_{\text{eq}} \rightarrow C7_{\text{ax}}$ transition by clustering all pathways sampled from the Action-CSA simulations (Figure 1A).

From the S_{OM} values obtained with different transition times (Figure 1B), it is clear that the pathway that passes barrier B has the lowest S_{OM} values along all transition times tested, which indicates that it is the most dominant pathway regardless of transition time. This is consistent with the LD simulation results. To compare the Action-CSA result with LD, we performed 5000 independent 100 ns LD simulations amounting to 500 μs trajectories (Table I). From the simulations, we observed 1350 transitions from $C7_{\text{eq}}$ to $C7_{\text{ax}}$ and categorized them by finding the nearest neighbor from the 8 pathways obtained with CSA. Among them, the pathway that crosses barrier B was identified as the most dominant one with all transition times. This demonstrates that Action-CSA correctly identified the minimum OM action pathway and that it matches the most dominant pathway observed in LD simulations.

TABLE I. The frequencies of pathways observed from 500 μs Langevin dynamics simulations.

Path ID	Frequency
Path1	1183
Path2	116
Path3	25
Path4	7
Path5	4
Path6	4
Path7	10
Path8	1

In addition, it is also identified that the Action-CSA simulations can provide information on the transition times of various pathways. Until $t < 0.8$ ps, the pathway that crosses barrier C (Path2) has the second lowest S_{OM} and the lowest S_{OM} value was observed at 0.4 ps. These are consistent with the LD results in which all 118 transitions that crossed barrier C occurred within 1.1 ps and their most probable transition time was 0.7 ps (the inset of Fig 1B). However, when $t > 0.8$ ps, Path3, which passes the fully extended conformation region $(\Phi, \Psi) = (-180^\circ, 180^\circ)$ and barrier A and B becomes the pathway with the second lowest S_{OM} . From the LD simulations, when $t > 0.9$ ps, 25 pathways similar to Path3 were

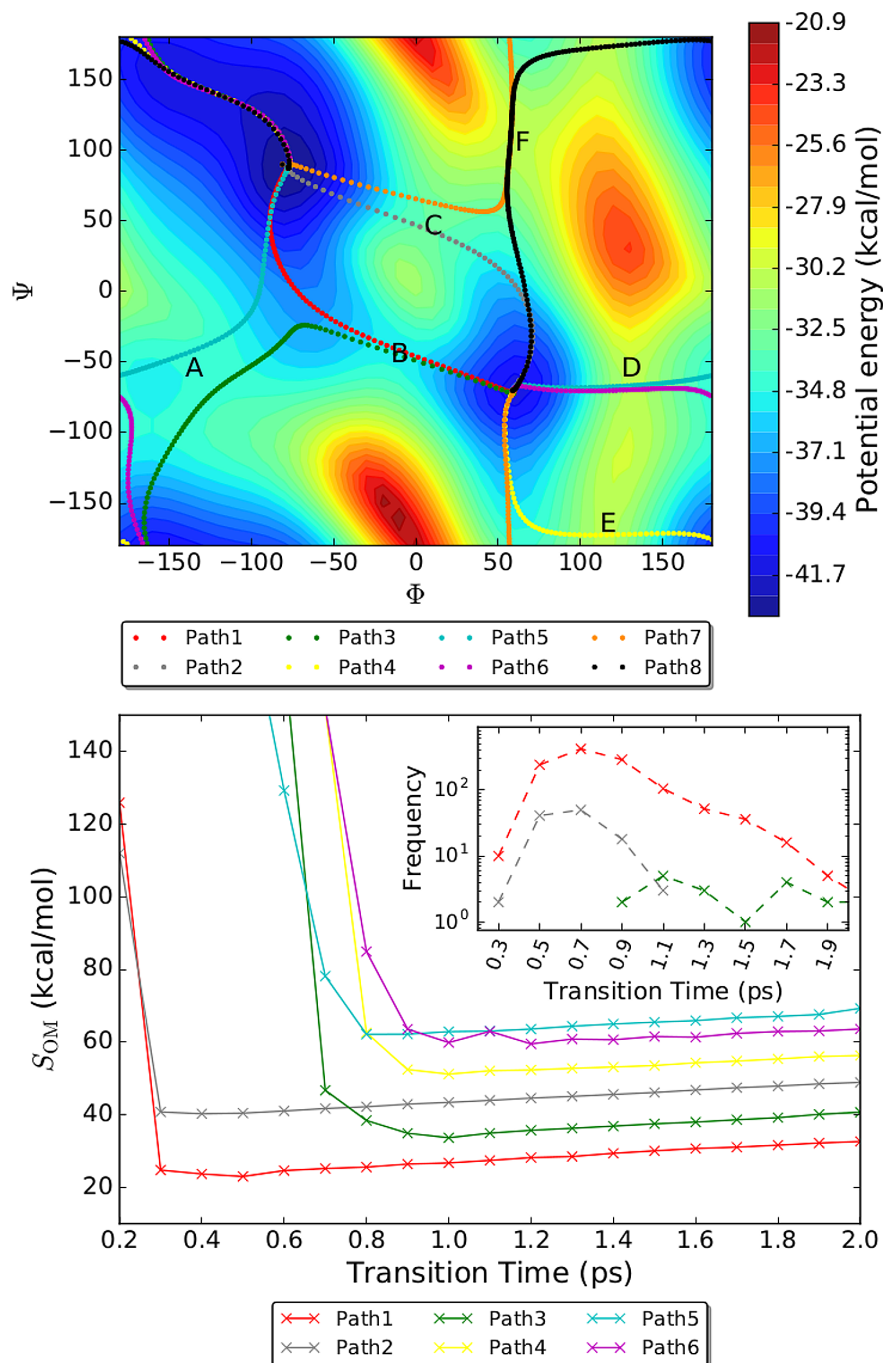


FIG. 1. Upper panel: eight different pathways for the $C7_{eq} \rightarrow C7_{ax}$ transition and the potential energy surface for the Φ and Ψ angles with the PARAM19 force field (in units of kcal/mol). Potential energy barriers are labeled in order of their heights (from A to F). Lower panel: the S_{OM} values of 6 pathways for the $C7_{eq} \rightarrow C7_{ax}$ transitions of alanine dipeptide along different transition times.

identified, which makes them the second dominant pathway. These results demonstrate that the profile of S_{OM} values is consistent with the distributions of transition times obtained from the LD simulations. Note that the most probable transition times observed from the LD simulations are longer than the minimum action transition times obtained from the CSA simulations. This is because high-frequency motions due to thermal fluctuations are filtered out in the minimum action pathways [1, 8, 9]. This means that the dwell time is well filtered out in the simulation, where a physically sufficient sampling time is assumed.

The second example is finding possible pathways for the conformational change of hexane from the all-gauche(-) (g-g-g-) to the all-gauche(+) state (g+g+g+). We assessed the sampling ability of Action-CSA by investigating how many low action pathways are found. If we assume that dihedral angles do not cross a high barrier around the *cis* state, all possible transition pathways between the two all-gauche states can be enumerated (Table II). For this reaction, there exist 44 possible pathways in total excluding cases where a torsional barrier is crossed multiple times. If the symmetries of dihedral angles and atomic order are considered, all 44 pathways can be categorized into 14 unique pathway types. We repeated the Action-CSA calculation of the reaction 40 times by using 200 trial pathways consisting of 100 replicas and a transition time of 3 ps.

In all simulations, the 6 lowest action pathways, C+C+, C-C-, T+C+, T+C-, C+M+, and C+M-, were found consistently. The other higher action pathways except for the highest action pathway, M+XM-, were found in at least 29 out of 40 CSA simulations. Only M+XM- was found in 9 simulations. On average, a single CSA simulation sampled 12 out of 14 unique path types and 26 out of 44 possible pathways. These results show that Action-CSA assuredly samples a number of lowest action, most dominant, pathways. The majority of the remaining pathways with higher actions can also be found with a tendency that relatively lower action pathways are more likely to be found. The sampling ability of Action-CSA can be improved by using a larger bank size. The potential energy landscape of the C+C+ pathway corresponding to the least S_{OM} shows that hexane crosses 6 energy barriers (Fig. 2). It should be noted that the fraction of possible pathways found on a given Action-CSA simulation depends on the number of replicas and the transition time. This example represents typical use, and not a best case scenario.

The third example is finding the folding pathway of FSD-1, a 28-residue mini-protein that has been widely investigated as a model system for studying protein folding [15, 49–52].

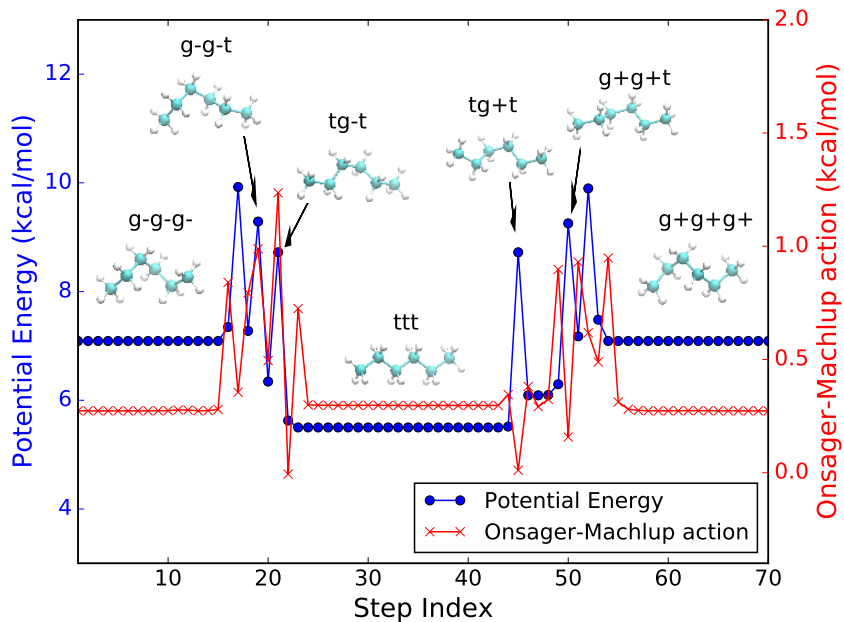


FIG. 2. The changes of potential energy and Onsager-Machlup action along the lowest action pathway between the all-gauche(-) to the all-gauche(+) conformations of hexane in the vacuum, the C+C+ pathway.

Folding pathways of FSD-1 from the fully extended conformation to the native structure were represented by using 100 replicas, a total folding time of 10 ps, and a temperature of 300 K. The protein was represented by the PARAM19 force field [47] and solvation effects were considered by the FACTS implicit solvent model [53]. This calculation required approximately 160 hours with 72 Haswell cores and diverse set of about twenty low action pathways were generated.

The characteristics of the identified lowest action folding pathway are consistent with experiments where the N-terminal β -hairpin is more flexible than the C-terminal α -helix [54]. A comparison of the RMSD values indicates that the α -helix folds first. Afterward, the folding of β -hairpin and the formation of hydrophobic core occur concurrently (the upper panel of Fig. 3). The potential energy landscape of FSD-1 folding shows that the potential energy decreases quickly after the 80th step suggesting that the step may be the transition state of folding (the lower panel of Fig. 3). The conformation at the 80th step shows that the helix is almost formed while the C-terminal region is not folded and the hydrophobic core is partially exposed, which is similar to transition states observed in previous conventional MD

simulations [49–52]. A detailed analysis of the other low action pathways for this system is beyond the scope of the letter, and will be explored as we examine the utility of this approach for use in examining how proteins fold.

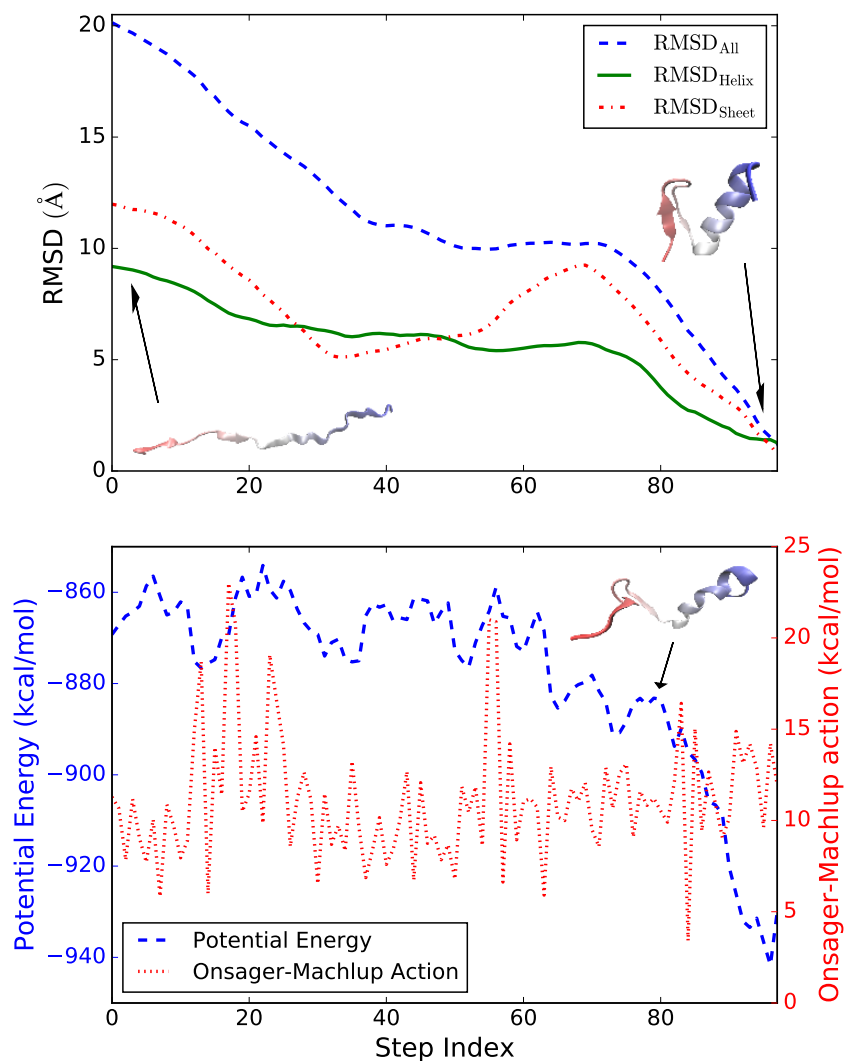


FIG. 3. Upper panel: The RMSD values of the entire FSD-1 (blue), the C-terminal α -helix (green, residue 14-28), and the N-terminal β -hairpin (red, residue 1-13) from the native structure along the folding pathway. Lower panel: The evolutions of potential energy (blue) and the Onsager-Machlup action (red) of FSD-1 along the folding pathway.

In conclusion, we demonstrated that efficient global optimization of Onsager-Machlup action reveals multiple reaction pathways successfully. In this work, we introduced a new computational method that samples not only the most dominant pathway but also other

possible pathways by optimizing Onsager-Machlup action using the CSA method. The advantages of our method over existing pathway sampling methods are the fact that it samples multiple pathways regardless of the quality of initial guesses on pathways; it requires only the calculation of first derivatives; and its sampling ability is not limited by high energy barriers separating pathways, which is a major limiting factor of previous MD-based pathway sampling methods in exploring pathway space [20, 22–26, 55]. In addition, we identified that the profile of minimum Onsager-Machlup actions found with different transition time parameters provide kinetic information on pathways. In terms of implementation, Action-CSA calculation is massively parallel because the local minimization of each trial pathway is independent of each other. Thus, pathway samplings for larger systems are readily possible with help of a large computer cluster system. We anticipate that the Action-CSA method will be used as a first-step exploration for complex reactions and large-scale conformational changes due to its low cost and robust nature. Results from Action-CSA can be used as the starting point for many other methods.

TABLE II: List of 14 unique pathway types and 44 non redundant pathways for conformational change of hexane from g-g-g- to g+g+g+.

Unique path type	Non redundant path
C+C+	g-g-g- \rightarrow tg-g- \rightarrow tg-t \rightarrow ttt \rightarrow tg+t \rightarrow tg+g+ \rightarrow g+g+g+
	g-g-g- \rightarrow g-g-t \rightarrow tg-t \rightarrow ttt \rightarrow tg+t \rightarrow g+g+t \rightarrow g+g+g+
C+C-	g-g-g- \rightarrow g-g-t \rightarrow tg-t \rightarrow ttt \rightarrow tg+t \rightarrow tg+g+ \rightarrow g+g+g+
	g-g-g- \rightarrow tg-g- \rightarrow tg-t \rightarrow ttt \rightarrow tg+t \rightarrow g+g+t \rightarrow g+g+g+
T+C+	g-g-g- \rightarrow tg-g- \rightarrow tg-t \rightarrow ttt \rightarrow ttg+ \rightarrow tg+g+ \rightarrow g+g+g+
	g-g-g- \rightarrow g-g-t \rightarrow tg-t \rightarrow ttt \rightarrow g+tt \rightarrow g+g+t \rightarrow g+g+g+
	g-g-g- \rightarrow g-g-t \rightarrow g-tt \rightarrow ttt \rightarrow tg+t \rightarrow g+g+t \rightarrow g+g+g+
	g-g-g- \rightarrow tg-g- \rightarrow ttg- \rightarrow ttt \rightarrow tg+t \rightarrow tg+g+ \rightarrow g+g+g+
T+C-	g-g-g- \rightarrow g-g-t \rightarrow tg-t \rightarrow ttt \rightarrow ttg+ \rightarrow tg+g+ \rightarrow g+g+g+
	g-g-g- \rightarrow tg-g- \rightarrow tg-t \rightarrow ttt \rightarrow g+tt \rightarrow g+g+t \rightarrow g+g+g+
	g-g-g- \rightarrow g-g-t \rightarrow g-tt \rightarrow ttt \rightarrow tg+t \rightarrow tg+g+ \rightarrow g+g+g+
	g-g-g- \rightarrow tg-g- \rightarrow ttg- \rightarrow ttt \rightarrow tg+t \rightarrow g+g+t \rightarrow g+g+g+

	$g-g-g- \rightarrow g-tg- \rightarrow ttg- \rightarrow g+tg- \rightarrow g+tt \rightarrow g+g+t \rightarrow g+g+g+$
M+XM-	$g-g-g- \rightarrow g-tg- \rightarrow g-tt \rightarrow g-tg+ \rightarrow ttg+ \rightarrow g+tg+ \rightarrow g+g+g+$
	$g-g-g- \rightarrow g-tg- \rightarrow ttg- \rightarrow g+tg- \rightarrow g+tt \rightarrow g+tg+ \rightarrow g+g+g+$

The authors wish to acknowledge helpful discussions with Attila Szabo and Richard Pastor. The research was supported by the Intramural Research Program of the NIH, NHLBI. Computational resources and services used in this work were provided by the LoBoS cluster of the National Institutes of Health.

* juyong.lee@nih.gov

- [1] R. Elber, *The Journal of Chemical Physics* **144**, 060901 (2016).
- [2] C. Dellago, P. G. Bolhuis, F. S. Csajka, and D. Chandler, *Journal of Chemical Physics* **108**, 1964 (1998).
- [3] P. G. Bolhuis, D. Chandler, C. Dellago, and P. L. Geissler, *Annual Review of Physical Chemistry* **53**, 291 (2002).
- [4] R. Czerminski and R. Elber, *International Journal of Quantum Chemistry* **186**, 167 (1990).
- [5] G. Henkelman, B. P. Uberuaga, and H. Jónsson, *Journal of Chemical Physics* **113**, 9901 (2000).
- [6] W. E, W. Ren, and E. Vanden-Eijnden, *Physical Review B* **66**, 5 (2002).
- [7] R. E. Gillilan and K. R. Wilson, *Journal of Chemical Physics* **97**, 1757 (1992).
- [8] R. Olender and R. Elber, *The Journal of Chemical Physics* **105**, 9299 (1996).
- [9] R. Elber, J. Meller, and R. Olender, *The Journal of Physical Chemistry B* **103**, 899 (1999).
- [10] R. Elber and D. Shalloway, *The Journal of Chemical Physics* **112**, 5539 (2000).
- [11] D. Passerone and M. Parrinello, *Physical Review Letters* **87**, 108302 (2001).
- [12] D. Passerone, M. Ceccarelli, and M. Parrinello, *Journal of Chemical Physics* **118**, 2025 (2003).
- [13] I.-H. Lee, J. Lee, and S. Lee, *Physical Review B* **68**, 064303 (2003).
- [14] I.-H. Lee, S.-Y. Kim, and J. Lee, *Chemical Physics Letters* **412**, 307 (2005).
- [15] I.-H. Lee, S.-Y. Kim, and J. Lee, *The Journal of Physical Chemistry. B* **116**, 6916 (2012).
- [16] I.-H. Lee, S.-Y. Kim, and J. Lee, *International Journal of Molecular Sciences* **14**, 16058 (2013).

- [17] R. Crehuet and M. J. Field, *Physical Review Letters* **90**, 089801; author reply 089802 (2003), arXiv:0104204v1 [arXiv:cond-mat].
- [18] L. Onsager and S. Machlup, *Physical Review* **91**, 1505 (1953).
- [19] S. Machlup and L. Onsager, *Physical Review* **91**, 1512 (1953).
- [20] P. Eastman, N. Grønbech-Jensen, and S. Doniach, *Journal of Chemical Physics* **114**, 3823 (2001).
- [21] D. M. Zuckerman and T. B. Woolf, *Physical Review. E, Statistical, nonlinear, and soft matter physics* **63**, 016702 (2000), arXiv:0005073v2 [arXiv:physics].
- [22] H. Fujisaki, M. Shiga, and A. Kidera, *Journal of Chemical Physics* **132**, 134101 (2010), arXiv:1003.0971.
- [23] H. Fujisaki, M. Shiga, K. Moritsugu, and A. Kidera, *The Journal of Chemical Physics* **139**, 054117 (2013), arXiv:1304.7342.
- [24] P. Faccioli, M. Sega, F. Pederiva, and H. Orland, *Physical Review Letters* **97**, 108101 (2006).
- [25] M. Sega, P. Faccioli, F. Pederiva, G. Garberoglio, and H. Orland, *Physical Review Letters* **99**, 118102 (2007).
- [26] S. Beccara, T. Skrbic, R. Covino, and P. Faccioli, *Proceedings of the National Academy of Sciences U.S.A.* **109**, 2330 (2012), arXiv:1111.3518v1.
- [27] J. Lee, H. Scheraga, and S. Rackovsky, *Journal of Computational Chemistry* **18**, 1222 (1997).
- [28] J. Lee, A. Liwo, and H. Scheraga, *Proceedings of the National Academy of Sciences U.S.A.* **96**, 2025 (1999).
- [29] J. Lee, I.-H. Lee, and J. Lee, *Physical Review Letters* **91**, 080201 (2003), arXiv:0307690 [cond-mat].
- [30] P. J. Steinbach, *Proteins: Structure, Function and Genetics* **57**, 665 (2004).
- [31] K. Joo, J. Lee, S. Lee, J.-H. Seo, S. J. Lee, and J. Lee, *Proteins* **69**, 83 (2007).
- [32] K. Joo, J. Lee, I. Kim, S. J. Lee, and J. Lee, *Biophysical Journal* **95**, 4813 (2008).
- [33] J. Lee, K. Joo, Kim, Seung-Yeon, and J. Lee, *Journal of Computational Chemistry* **29**, 2479 (2008).
- [34] K. Joo, J. Lee, J.-H. Seo, K. Lee, B.-G. Kim, and J. Lee, *Proteins: Structure, Function, and Bioinformatics* **75**, 1010 (2009).
- [35] J. Lee, J. Lee, T. N. Sasaki, M. Sasai, C. Seok, and J. Lee, *Proteins: Structure, Function, and Bioinformatics* **79**, 2403 (2011).

- [36] J. Lee, S. P. Gross, and J. Lee, *Physical Review E* **85**, 056702 (2012).
- [37] J. Lee and J. Lee, *PLOS ONE* **8**, e60372 (2013).
- [38] J. Lee, S. P. Gross, and J. Lee, *Scientific Reports* **3**, 2197 (2013).
- [39] B. R. Brooks, C. L. Brooks, A. D. Mackerell, L. Nilsson, R. J. Petrella, B. Roux, Y. Won, G. Archontis, C. Bartels, S. Boresch, A. Caffisch, L. Caves, Q. Cui, A. R. Dinner, M. Feig, S. Fischer, J. Gao, M. Hodoscek, W. Im, K. Kuczera, T. Lazaridis, J. Ma, V. Ovchinnikov, E. Paci, R. W. Pastor, C. B. Post, J. Z. Pu, M. Schaefer, B. Tidor, R. M. Venable, H. L. Woodcock, X. Wu, W. Yang, D. M. York, and M. Karplus, *Journal of Computational Chemistry* **30**, 1545 (2009).
- [40] K. Joo, I. Joung, J. Lee, J. Lee, W. Lee, B. Brooks, S. J. Lee, and J. Lee, *Proteins: Structure, Function and Bioinformatics* **83**, 2251 (2015).
- [41] K. L. C. Hunt and J. Ross, *The Journal of Chemical Physics* **75**, 976 (1981).
- [42] A. B. Adib, *The Journal of Physical Chemistry. B* **112**, 5910 (2008), arXiv:0712.1255.
- [43] K. R. Haas, H. Yang, and J. W. Chu, *Journal of Physical Chemistry Letters* **5**, 999 (2014).
- [44] K. R. Haas, H. Yang, and J. W. Chu, *Journal of Physical Chemistry B* **188**, 8099 (2014).
- [45] T. F. Miller and C. Predescu, *Journal of Chemical Physics* **126**, 144102 (2007).
- [46] H. Alt and M. Godau, *International Journal of Computational Geometry & Applications* **05**, 75 (1995).
- [47] E. Neria, S. Fischer, and M. Karplus, *The Journal of Chemical Physics* **105**, 1902 (1996).
- [48] R. J. Loncharich, B. R. Brooks, and R. W. Pastor, *Biopolymers* **32**, 523 (1992).
- [49] S. Jang, S. Shin, and Y. Pak, *Journal of the American Chemical Society* **124**, 4976 (2002).
- [50] H. Lei and Y. Duan, *Journal of Chemical Physics* **121**, 12104 (2004).
- [51] H. Lei, S. G. Dastidar, and Y. Duan, *Journal of Physical Chemistry B* **110**, 22001 (2006).
- [52] C. Wu and J. E. Shea, *PLoS Computational Biology* **6**, e1000998 (2010).
- [53] U. Haberthür and A. Caffisch, *Journal of Computational Chemistry* **29**, 701 (2008).
- [54] J. A. Feng, J. Kao, and G. R. Marshall, *Biophysical Journal* **97**, 2803 (2009).
- [55] D. H. Mathews and D. A. Case, *Journal of Molecular Biology* **357**, 1683 (2006).